In vitro long term differentiation and functionality of three-dimensional bioprinted primary human hepatocytes: application for in vivo engraftment

Marie Cuvellier, Sophie Rose, Frédéric Ezan, Ulrich Jarry, Hugo de Oliveira, Arnaud Bruyère, Christophe Drieu La Rochelle, Vincent Legagneux, Sophie Langouët, Georges Baffet

In vitro long term differentiation and functionality of three-dimensional bioprinted primary human hepatocytes: application for *in vivo* engraftment

Marie Cuvellier[1]*, Sophie Rose[1]#, Frédéric Ezan[1]#, Ulrich Jarry[2,3], Hugo de Oliviera[3], Arnaud Bruyère[1], Christophe Drieu La Rochelle[3], Vincent Legagneux[1], Sophie Langouët[1]*, Georges Baffet[1]*

[1]Univ Rennes, Inserm, EHESP, Irset (Institut de recherche en santé, environnement et travail) - UMR_S 1085, Rennes, France
[2]Univ Rennes, CNRS, INSERM, BIOSIT UAR 3480, US_S 018, Oncotrial, F-35000 Rennes, France
[3]Biotrial Pharmacology, Unité de Pharmacologie Préclinique, Rennes, France
[3]Univ Bordeaux, ART Bioprint, Inserm – UMR 1026, Bordeaux, France

*Corresponding authors
#These authors contributed equally to this work

Corresponding authors:
Georges Baffet, UMR 1085, IRSET, Inserm-University of Rennes 1, Campus de Villejean, CS 34317, 35043 Rennes, France. E-mail: georges.baffet@univ-rennes1.fr
Sophie Langouët, UMR 1085, IRSET, Inserm-University of Rennes 1, Campus de Villejean, CS 34317, 35043 Rennes, France. Tel: (33)2.23.23.36.08. E-mail: sophie.langouet@univ-rennes1.fr
Marie Cuvellier, UMR 1085, IRSET, Inserm-University of Rennes 1, Campus de Villejean, CS 34317, 35043 Rennes, France. E-mail: marie.cuvellier@univ-rennes1.fr

Received xxxxxx
Accepted for publication xxxxxx
Published xxxxxx

Abstract

In recent decades, 3D *in vitro* cultures of primary human hepatocytes (PHH) have been increasingly developed to establish models capable of faithfully mimicking main liver functions. The use of 3D bioprinting, capable of recreating structures composed of cells embedded in matrix with controlled microarchitectures, is an emergent key feature for tissue engineering. In this work, we used an extrusion-based system to print PHH in a methacrylated gelatin matrix (GelMa). PHH bioprinted in GelMa rapidly organized into polarized hollow spheroids and were viable for at least 28 days of culture. These PHH were highly differentiated with maintenance of liver differentiation genes over time, as demonstrated by transcriptomic analysis and functional approaches. The cells were polarized with localization of apico/canalicular regions, and displayed activities of phase I and II biotransformation enzymes that could be regulated by inducers. Furthermore, the implantation of the bioprinted structures in mice demonstrated their capability to vascularize, and their ability to maintain human hepatic specific functions for at least 28 days was illustrated by albumin secretion and debrisoquine metabolism. This model could hold great promise for human liver tissue generation and its use in future biotechnological developments.

Keywords: 3D culture, 3D bioprinting, primary human hepatocytes, tissue engineering, methacrylated gelatin

1. Introduction

The central role of the liver in the metabolism of xenobiotics makes parenchymal cell cultures essential *in*

vitro models for understanding and analyzing detoxification functions [1]. The last decades, primary cultures of rodent and human hepatocytes in 2D cultures have been widely developed by numerous laboratories. However, rodent hepatocytes cultivated in 2D fail to develop a normal tissue architecture, resulting in the rapid loss of many tissue-specific functions after one week of culture [2]. Primary human hepatocytes (PHH) cannot survive for more than two weeks in 2D cultures and rapidly lose their differentiated functions [3], [4]. In addition, because of specific biotransformation variabilities between rodent and human metabolism enzymes, results from drug toxicity assays performed with animals are not always transposable to human [5].

In vitro 3D spheroid cultures of PHH appear to be particularly suited for maintaining PHH with a stable phenotype, morphology and viability over prolonged culture periods [6]–[10] while cells grown in conventional 2D monolayers rapidly lose their differentiated characteristics and have a lower survival potential [3], [4]. This superiority of 3D models to maintain hepatocyte-specific functions warrants their use to study the biotransformation of xenobiotics [8], [10]–[12] and is generating increasing interest in biotechnology developments for drug safety or efficacy prescreening tests and for regulatory purposes as an alternative to animal testing. In parallel, 3D cell culture models of PHH embedded in matrix such as including alginate [13], Matrigel [14]–[16], or collagen [9], [17], [18] have been widely developed and optimized in the last decade to more accurately reflect *in vivo* physiology and enable the maintenance of tissue specific functions. These matrices, by mimicking the physico-chemical properties of the human extracellular matrix, provide the mechanical support, physical structure and chemical signaling needed for the hepatocytes homeostasis and differentiation [17], [19], [20] Indeed, their rigidity, much closer to that of the human liver than that of plastic supports, modulates their phenotype and their responses to growth factors via the signaling pathways associated with junction proteins such as integrins [21], [22]. Moreover, the presence of RGD- domains found in matrices of mammalian origin promotes cell adhesion and viability [23], [24], and the scaffold they recreate allow the cells to attach in 3D, thus increasing the number of possible cell-cell interactions compared to 2D culture [19]. We have previously shown the value of combining spheroids and matrix by using the establishment of 3D cell-cell interactions followed by encapsulation of the cell cluster in collagen matrix to culture hepatocytes, including PHH [9], [17], [25]. This technique promotes a favorable environment for the establishment of PHH spheroids, enabling them to remain differentiated and proliferating over a prolonged period.

In this context, 3D bioprinting of hepatocytes is particularly attractive because of its ability to pattern structures in 3D. This biotechnology allows the precise deposition of cells embedded in hydrogels, thus enabling the obtention of complex 3D structures. Bioprinting has shown great potential in tissue bioengineering, whether through its ability to provide prevascularized structures [26], to recreate structures comprising different types of hepatic cells in co-culture [27], [28], or to precisely control the architecture of structures incorporated into microfluidic systems [29]. Numerous bioprinted liver models, using hepatic cell lines [25], [29]–[34], induced pluripotent stem cells (iPSC) [28], [35], [36] or primary rodents hepatocytes [37] have been developed over the last years. However, the use of hepatic cell lines is limited by their dedifferentiation compared from the human hepatocyte phenotype, and cells of animal origin are unrepresentative due to interspecies differences. iPSCs represents an important hope in the generation of human hepatocytes, it should be noted that their differentiation has long remained limited to the fetal stage, and their full differentiation to a hepatocyte level, requiring a long and complex protocol, has been only recently demonstrated [38]. Despite the promising advantages of bioprinting to produce advanced structures for the 3D culture of hepatocytes, to date there is no easily available model of PHH bioprinting. As of yet, Organovo (San Diego, USA) and Cyfuse Biomaterials (Tokyo, JP) are the only companies that have succeeded in bioprinting PHH in mono- [39] or co-cultures with human stellate cells [40] and umbilical cord endothelial cells (HUVECs) [27], [41]. Their models recreate an architectural environment resembling liver tissue *in vivo*, that can support liver and metabolic functions for more than a month. Due to the pre-bioprinting recreation of cellular contacts prior bioprinting, and the high cell concentration, the reconstituted models are histologically close to human tissue *in vivo*.

However, the use of these bioprinting approaches to obtain an *in vitro* liver model is severely limited. Those models are bioprinted by private companies, with proprietary bioprinters and very limited information on the protocols used. The impossibility of using this model outside the framework of private enterprise and their cost limits their broader use by other research actors.

Here, we propose a detailed protocol (matrix composition, printing parameters, bioprinted structures) allowing the reproduction of the results obtained by any team equipped with a lower cost bioprinter meeting aforementioned bioprinting criteria. The bioprinting of PHH poses many technical challenges; many parameters relating to the bioprinting technique, as well as to the ink used, must be determined in order to obtain bioprinted structures which are stable and viable over time. Indeed, multiple parts of the bioprinting process, such as viscosity of gels, stress exerted by extrusion and plotting [42], harmful wavelengths and free radicals generated by photo-initiators can greatly affect short- and long-term cell viability [43], [44]. Moreover, bioprinting naturally derived cell-laden hydrogels can be challenging due to their poor mechanical properties [45].

Here, we combined methacrylated gelatin (GelMa) with PHH aggregates to produce a cellular liver model by extrusion bioprinting. GelMa is a low-cost, widely available and easy to utilize matrix [46], which has recently been used successfully by extrusion or stereolithographic printing of the hepatic HepaRG cell line [25], [30] or of induced pluripotent stem cells [28]. In a recent report, we defined the optimal conditions for bioprinting and preserving long-term viability of HepaRG in GelMa, using an extrusion technique. We demonstrated that bioprinted HepaRG cells had long-term viability (> 28 days) with a differentiated phenotype and functions equivalent or superior to those of the gold standard in 2D-DMSO [25].

Based on the protocols developed for this hepatic cell line, we assessed whether GelMa could support the long-term viability and liver function of PHH to generate a potential *in vitro* model for metabolism and hepatotoxicity studies. Histological, transcriptional and functional characterizations of the 3D bioprinted PHH were performed. The cells quickly organized in hollow spheroids and displayed very defined apical and basal polarities. Bioprinted PHH were able to maintain viability and liver specificity for at least one month of culture. Here, we present the first bioprinted model of differentiated, proliferative PHH, named Hepoid in GelMa, using easily available matrix and printing extrusion technology. Furthermore, after engraftment in mice, the vascularized structures released human albumin and produced a specific metabolite of human CYP2D6 that could be measured in the serum of the mice for at least 28 days. Altogether, our findings demonstrate that this model would be suitable for future biotechnological developments and tissue engineering.

2. Material and Methods

2.1 Reagents

William's E medium and TRIzol were purchased from Invitrogen (Invitrogen, Carlsbad, CA, USA). FBS and sacharrose were purchased from Eurobio (Evry, France). Penicillin/ Streptomycin were purchased from Thermo Fisher (Waltham, MA USA). WST1, Bovine serum albumin, Human insulin, ITS (insulin, transferrin, selenium), hydrocortisone hemisuccinate, liberase (05401020001), DMSO (D4540), oleic acid (O1383), stearic acid (S4751), amiodarone, formaldehyde, gelatin, 5-ethylnyl-2'-deoxyuridine (EdU), salicylamide, CY5-azide, ethoxyresorufin and methyresorufin, 3- methylcholanthrene (3MC) and rifampicin were purchased from Sigma-Aldrich (St. Louis, MO, USA). Methacrylated gelatin (GelMa) was synthesized by the ART Bioencres (Bordeaux, FR). Lithium phenyl-2,4,6 trimethylbenzoylphosphinate (LAP) was purchased from TCI (Japan). rhHGF was purchased from R&D systems (Minneapolis, USA) while rhEGF was purchased from Promega (Madison, USA). Phenobarbital was provided by the Coopération pharmaceutique française. The Dapi Fluoromount- G™ was purchased from Southern Biotech (Birmingham, AL, USA). Debrisoquin sulfate, 4OH-debrisoquine were purchased from Santa Cruz Biotechnology, Heidelberg, DE)

2.2. Cell culture

2.2.1.Cell isolation and 2D culture

Primary human hepatocytes (PHH) were obtained from patients undergoing liver resection through the Centre de Ressources Biologiques (CRB) Santé of Rennes (CHRU Pontchaillou, Rennes, FR, http://www.crbsanterennes.com) and approved by the Inserm Ethical Review Committee (October 8, 2013-IRB00003888). Freshly isolated human hepatocytes were obtained from the histologically normal part of the biopsy and isolated by a two-step collagenase perfusion procedure as described previously. The research protocol was conducted under French legal guidelines and the local institutional ethics committee. Written informed consent was obtained from all donors of liver material. Cryopreserved PHH were obtained from Biopredic International (Rennes, FR) or Cytes Biotechnologies (Barcelona, SP). For 2D cultures, cells were seeded in MW96 plates at a density of 4.5×10^4 cells/well in William's medium supplemented with bovine serum albumin (1 g/l), glutamine (2 mM), bovine

insulin (5 µg/ml), penicillin (100 U/ml), streptomycin (100 µg/ml) and fetal bovine serum (FBS) (10% v/v). The culture medium was renewed with hydrocortisone hemisuccinate 54 µM without FBS. In order to promote the establishment of cell–cell interactions and the formation of cell clumps which were then to be embedded into the GelMa matrix, fresh or cryopreserved hepatocytes were first incubated overnight (i.e., 12–15 h) in ultra-low-attachment plate (ULAP) (Corning Costar) at a concentration of 2×10^6 cells/well of a MW6 plate in the medium described previously before being embedded in the GelMa matrix. Comparisons between 2 conditions (2D vs 3D and FBS+ vs FBS-) were performed using hepatocytes from the same donor for each condition, in technical triplicate.

2.2.2.Bio-Ink preparation and bioprinting process

GelMa was synthesized as previously described by Loessner et al. [46]. A 10% (w/v) gelatin (Type A, 300 bloom from porcine skin, Sigma) solution in PBS, was heated at 60°C for 2h with stirring. Next, the temperature was adjusted to 50°C and methacrylic anhydride (Sigma) was added drop-wise at 0.14 mL/g of gelatin. The solution was left to react for 4h while stirring, then diluted to with PBS 5% (w/v). The methacrylated gelatin was precipitated in a 4-fold excess volume of cold acetone. Precipitated gelatin was recovered, vacuum dried for 30 min then redissolved in 40°C PBS 10% (w/v). Then, gelatin was dialyzed for 3 days using a 12–14 kDa molecular weight cutoff (MWCO) dialysis tubing (Sigma), against deionized water with 2 daily water changes. Once purified, GelMa was frozen at 80°C, freeze-dried and stored at 20°C. by By TNBS assay, methacrylation degree was determined to be 60.4 ± 1.4% (n = 3). For bio-ink preparation, GelMa was dissolved overnight in William's E medium at 37°C. Then, lithium phenyl-2,4,6 trimethylbenzoylphosphinate (LAP) previously dissolved in PBS (10 mg/mL) was added at 0.1 % (w/v) concentration and the cells were added to the final suspension. The final cell-laden bio-ink was composed of 5 % (w/v) GelMa, 0.1 % (w/v) LAP, 1×10^6/mL PHH.

The 3D constructs were designed by the computer aided design software OnShape (Cambridge, MA, USA). For the bioprinting process, the ink was put in an extruder maintained at 20°C and the bio-ink was extruded through a 23 G needle at 1.4 – 2.4 bar, 240 mm/min, with the extrusion printer Allevi 2 (Allevi, Philadelphia, PA, USA). Macroscopic imaging and CAD design of the structures are illustrated in. Figure 1. As previously described [25], *in vitro* studies were performed with 7×7×2 mm (± 100 µL) cuboidal gels extruded into multiwell 48 plates while the structures used for *in vivo* reimplantation (11.4×11.4×2 mm, ± 200 µL) were grown in multiwell 24 plates.

The bioprinted constructs were exposed to violet light during 1 min at 405 nm, 7 mW/cm^2, in order to induce crosslinking of GelMa. They were then cultured in a 3D culture medium described previously supplemented with hydrocortisone hemisuccinate 1.08 µM, ITS (Recombinant insulin 10 µg/ml, transferrin 5.5 µg/ml, sodium selenite 5 ng/ml) (Sigma-Aldrich), rhHGF (2.5 ng/ml) (BioLegend) and rhEGF (50 ng/ml) (PeproTech). The medium was renewed every 48–72 h. This method of culture is protected under an international patent (EP20180305603201805l6 / WO2019219828) [9], [25], [47]

2.3. Immunostaining

Bioprinted structures were fixed in 4% formaldehyde, washed 3x in PBS and suspended in a phosphate buffer 0.12 M with sucrose 10% (w/v) and incubated overnight. They were impregnated with a cryoprotective matrix composed of gelatin 7.5% (w/v) and sucrose 10% (w/v), then frozen at -80°C 1 min in isopentane and cryosectionned at a 4 µm thickness. The Discovery Automated IHC stainer using the discovery Rhodamin kit (Ventana Medical Systems, Tucson, AZ, USA) was used to stain the slides. The concentrations and references of used primary antibodies canbe found in Supplemental Table 1. The slides were rinced and signal enhancement was carried out using the Ventana Rhodamin kitand secondary antibody anti-rabbit HRP (760–4311, Roche) or secondary antibody anti-mouse HRP (760–4310, Roche) for incubation during 16 min. The slides were then manually rinsed, stained with albumin antibody then with a secondary antibody for albumin detection (Donkey anti goat 488), and mounted using Dapi Fluoromount- G™. The imaging was processed using a fluorescence Eclipse Ni-E microscope (Nikon) equipped with a photonic camera Orca R2 (Hamamatsu). ImageJ software (National Institutes of Health, http://imagej.nih. Gov/ij/) was used to carry out image processing.

2.4. Cell viability assay

Cell viability was assessed by a Zombie NIR labelling using a Zombie Dye Viability Kit (Biolegend, JP) following the manufacturer protocol. Briefly, cells

suspensions and bioprinted structures were washed by PBS and stained 30 min at RT by a 1:2000 Zombie dye solution. They were then washed by a PBS/BSA 1% solution. For bioprinted structures, GelMa degradation was carried by a 2h30 incubation in liberase 10 µg/mL at 37°C in order to recover the embedded PHH. Cells were spread in a superfrost slide, mounted with Dapi Fluoromount-G™ and the staining was monitored using a fluorescence microscope (Eclipse Ni-E, Nikon, Amsterdam, NL).

2.4. Proliferation estimation

For EdU incorporation, cell-laden constructs were treated 48h with EdU at 10 µM. Constructs were then fixed and cryosectionned as described in the *Immunostaining* M&M section. Slides were permeabilized using Triton X-100 0.1% (v/v) for 10 min. They were then treated for 1h with a mix of ascorbic acid (0.1 M), Tris pH 8.5 (0.1 M), CuSO4 (1 µM) and CY5-azide (1.5 µM, Sigma) for 1h. The slides were mounted using the Dapi Fluoromount- G™ and the cell nucleus staining was detected using a fluorescence microscope (Eclipse Ni-E, Nikon, Amsterdam, NL). ImageJ software (National Institutes of Health, http://imagej.nih. Gov/ij/) was used to carry out image processing and nucleus counting.

2.5. RNA extraction and quantitative real time PCR

At the specified time points in culture, cell-laden structures were harvested, washed twice in PBS and total RNAs were extracted using TRIzol. The concentration of total RNAs were measured with a NanoDrop ND-1000 (NanoDrop Technologies). cDNA was synthesized using the High Capacity cDNA reverse transcriptase kit (Applied Biosystems Foster City, CA, USA), and Real-time PCR was performed using the Power SYBR Green PCR master mix (Applied Biosystems Foster City, CA, USA). Primer-BLAST (NCBI USA), was used to design primer sequences which were purchased from Eurogentec (Searing, BE). All used primers are listed in Supplemental Table 2. The amplification curves were analyzed with the Bio-Rad CFX Manager software using the comparative regression method. GAPDH was used for the normalization of expression data. The relative amount of measured mRNA in samples was determined using the 2- ΔΔCT method where $\Delta\Delta CT = (Ct_{target} - CT_{GAPDH})$ sample- $(Ct_{target} - CT_{GAPDH})$ calibrator. Results were expressed as the n-fold difference of target gene expression in samples as compared with the mean expression value of the 2D cultures used as calibrator.

2.6. Transcriptomic analysis

Total RNAs were obtained and purified from freshly isolated human hepatocytes (PHH T0) (n = 5), from PHH at day 4 of culture in 2D (PHH 2D D4) (n=5) and from PHH on GelMa at day 14 of culture (PHH 3D D14) (n=4). The samples were concentrated using the RNA Clean & Concentrator-5 (Zymo, Irvine, CA, USA) and checked for RNA degradation based on the RNA Integrity Number (RIN>6). 3' sequencing RNA Profiling (3′ SRP-seq) libraries were made at the GenoBIRD facility of Nantes, France, and sequenced using the HiSeq 2500 (Illumina, San Diego, CA, USA) following the described protocol in Soumillon, bioRxiv 003236 (2014). The analysis of the generated data was performed using R packages. The differentially expressed genes ($FC > 2$, $p < 0.05$) between the different conditions (i.e., PHH 2D and PHH 3D vs T0 and PHH 2D vs PHH 3D) were functionally analyzed using the WEB-based database GeneSeT AnaLysis Toolkit (WebGestalT), restricted to protein coding data set, by computing enrichments for gene ontology (GO) terms. The data were then selected as the top ten of the enriched categories, sorted by increasing enrichment ratios (FDR <0.05).

2.7. Metabolic analysis

For 3D and 2D culture of PHH, 24h medium samples were taken for the determination of albumin and urea content at specific culture time points. Secreted albumin was quantified using the human serum albumin Duoset Enzyme Linked Immunosorbent Assay (ELISA) kit (R&D systems, MN, USA), following the manufacturer's instructions. The absorbance at 450 nm was mesured using a microplate reader (SpectrostarNano, BMG Labtech, Champigny s/Marne, Fr) and used to quantify albumin concentration. Urea secretion in the medium was measured using A ChromaDazzle Urea Assay kit (AssayGenie, Dublin, IR) was used to quantify urea secretion in the culture medium, according to manufacturer's protocol, reading the absorbance at 420 nm using a microplate reader (SpectrostarNano, BMG Labtech, Champigny s/Marne, Fr).

2.8. CYP activity measurements by luminescence

CYP1A2, 2B6, 2C9 and 3A4 activities were assessed by treating cells with DMSO 0.1 % v/v for basal activities. Induction of CYP was performed by treating with 3MC (5 µM, 24h) (CYP1A2), phenobarbital (0.2 mM, 72h)

(CYP2B6) or rifampicin (5 µM, 72h) (CYP2C9 and CYP3A4). CYPs activities were assessed using the P450 GloAssay (Promega) following to the manufacturer's instructions. Briefly, a Luciferin CYP specific substrate was added on bioprinted structures and they were incubated at 37°C. After 1 h (CYP1A2, CYP2B6 and CYP3A4) or 4h (CYP2C9) of incubation, the CYP-induced conversion of Luciferin substrate to Luciferin was determined. The supernatant was incubated with Luciferin detection reagent during 20 min at RT and luminescence was measured after which normalization of activity with the quantity of viable cells was assessed by a WST1 test.

2.9. TPEF microscopy

Imaging with TPEF microscopy was performed at the Mric facility of Biosit, University of Rennes1 (Fr). The TPEF imaging system is composed of a confocal TCS SP5 scanning head (Leica Microsystems, Mannheim, Germany), which is mounted on a DMIRE2 inverted microscope (Leica Microsystems). It was equipped with a Multiphoton Ma Ta HP Ti: Sapphire Mode Locked Laser (Spectra Physics, Santa Clara, CA) used to excite the samples at 810 nm. A 20x oil immersion and a 60x water immersion objective (Olympus LUMFL 60W x 1.1NA) were used. The TPEF was epi-collected in the backward direction. IRSP 715 bandpass and 405 nm infrared (IR) filters (10 nm full width at half-maximum, FWHM) were placed before the photomultiplier tube. Image processing was performed with ImageJ software (National Institutes of Health, (http://imagej.nih. Gov/ij/)).

2.10. In vivo experiments

NSG (NOD.Cg-Prkdc^{scid} Il2rg$^{tm\ Wjl}$ / SzJ) mice were purchased from Charles River Laboratories (Wilmington, MA). 3D structures were printed as described in Fig.7A and loaded with 2×10^6/mL cryopreserved PHH from 3 different donors (Supplemental Table 3). Sham structures were bioprinted in the same conditions with GelMa without cells. 3 structures were bioprinted for each donor. Bioprinted structures were kept 7 days in 3D culture medium prior to engraftment. The experiments were performed using 12 NSG mice (7 males, 5 females) which were randomly split among the four groups (PHHA, PHHB, PHHC, Sham), with 3 mice in each group. Structures were implanted subcutaneously. The mice were euthanized after 4 weeks to collect blood and the engrafted samples. 30 min prior to sacrifice, they were given debrisoquine (DEB) at 4mg/kg *per os*. Serum was separated from blood and human albumin was dosed using the protocol described in the Metabolic analysis section. Liquid chromatography-tandem mass spectroscopy (LC-MS/MS), based on a high performance liquid chromatography Aria system (Agilent, Les Ulis, France), equipped with a Poroshell 120 C18 (4.6 x 150 mm) column (Agilent, Les Ulis, France) and coupled to a tandem mass spectrometry TSQ Quantum Ultra (Thermo Fisher Scientific, Villebon sur Yvette, France), fitted with an electrospray ionization source (ESI+), was additionally used for analyzing DEB and its human specific CYP2D6 metabolite 4-hydroxydebrisoquine (4OH-DEB). Monitored ion transitions were at 176.1 > 159.1 and 192.1 > 132.2 (m/z) for DEB and 4OH-DEB, respectively. The engrafted scaffolds were collected and processed as described in the Immunostaining and TPEF imaging sections.

2.11. Statistical analysis

Unless otherwise specified in the legends, all data shown are expressed as means ± standard deviations (SDs) of n=3 different experimentations using PHH from different donors. Student t-test or one-way analysis of variance (ANOVA) were used for the evaluation of the difference between the mean values in each group (GraphPad Prism 6, GraphPad Software, Inc.; La Jolla, CA, USA). Significant differences for p-value thresholds are represented as followed: $p \leq 0.05$ (*); $p \leq 0.01$ (**); $p \leq 0.001$ (***), $p \leq 0.0001$ (****).

3. Results

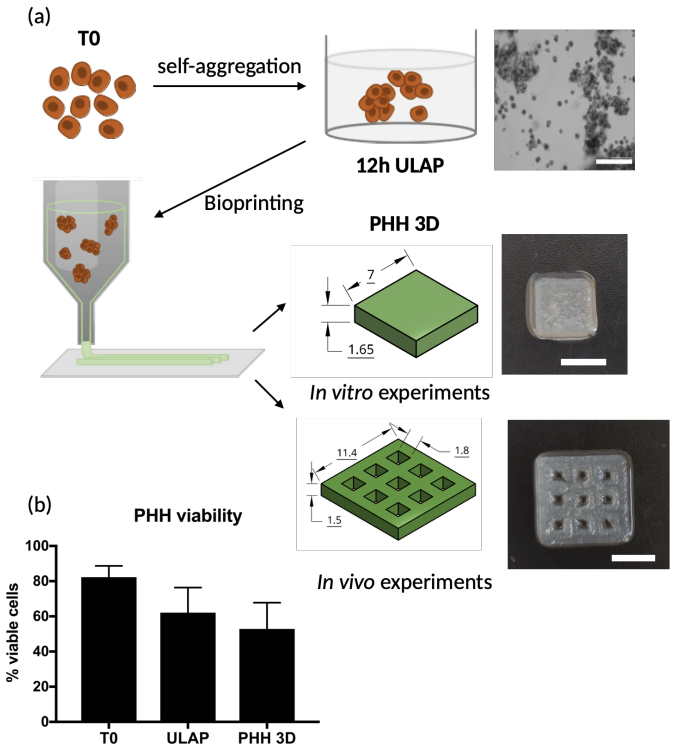

Figure 1 : schematic representation of the experimental workflow

(a) The PHHs are set to auto-aggregate overnight in ultra-low attachment plate (ULAP). Right : Macroscopic imaging of PHHs after 12h self-aggregation. Scale bar= 100 µm. The aggregates are recovered, included in a GelMa matrix and bioprinted by extrusion. Two models, one for in vitro *experimentation and the other for* in vivo *reimplantation, were bioprinted. Lengths of CAD drawings are given in mm. Scale bar of macroscopic images of structures : 5 mm. (b) Viability measurement of PHH before ULAP (T0), after 12h ULAP (ULAP) and 24h after bioprinting (PHH 3D).*

3.1. PHH in GelMa are organized into polarized hollow spheroids and have long-term viability

We have previously defined a bioprinting protocol [25] allowing long term viability and functionality of cultured cells, that we applied in the present work to the bioprinting of primary adult human hepatocytes. Freshly isolated PHH were first plated on a low attachment plate (ULAP) for 12 hours to enhance cell-cell interactions before seeding in 3D cultures as recently described by Rose et al [9]. Then, small clusters of PHH were printed in 5% GelMa with an extrusion bioprinter, forming 7×7×2 mm structures as illustrated in Figure 1(a). Cell viability was carried estimated in order to measure the impact of the different steps of the workflow on the PHH. A 24.33 ± 16.74% mortality was detected after the 12h ULAP step and, 24h after bioprinting, viability was further reduced by 15.49 ± 5.58% (Figure 1(b)). During bioprinting, several factors can directly impact cell viability: the most important identified are LAP concentration, lighting and extrusion shear stress. The impact of the latter in particular has been discerned by comparing in parallel the viability of PHHs in GelMa, either simply cast in molds and lighted, or bioprinted according to our protocols. The viability study showed that of the 15.49 ± 5.58 % decrease in viability observed, only 6.07 ± 0.27 % could be attributed to bioprinting stress and the remaining 9.41 ± 5.79% to LAP concentration and lighting. (Supplementary Figure 1).

After bioprinting in GelMa, PHH 3D organization evolved during culture. As showed in Figure 2(a) and 2(b), immediately after bioprinting (Day 0), PHH are homogeneously distributed in the bioprinted gels, as cells aggregates. A progressive organization is set up along the culture and their organization in hollow spheroids can be clearly visualized 14 days after seeding (Figure 2(b)). The morphology and organization of PHH 3D in GelMa was also observed by two-photon excitation fluorescence (TPEF) microscopy. After Z-stack reconstruction, TPEF scanning of bioprinted structures performed at day 14 allowed the detection of cell spheroids throughout the GelMa (Figure 2(b)) and 3D reconstruction of structures is shown in the supplemental video.

Measurement of the size of the Alb+ positive clusters, as well as z-projection of TPEF stacks of the structures, showed that the organization in spheroids is not concomitant with an increase in spheroids size through the whole 28 days of culture (respective mean diameters at days 0 = 74.13 ± 27.51 µm and day 14 = 84.56 ± 28.54 µm) (data not shown).

The hollow spheroid organization was concomitant with the polarization of PHH 3D. The cells appeared highly polarized as assessed by the localization of E-cadherins, N-cadherins and vimentin on the apical and lateral membranes at days 7, 14 and 28 after bioprinting (Figure 2(c)). We then compared the mRNA expression of those markers to those of PHH from the same donors, analyzed on day 7 of 2D cultures. Interestingly, mesenchymal markers such as CDH2 (N-cadherin) and VIM appeared to be expressed at very low levels compared to 2D cultures, while CDH1 (E-cadherin), an epithelial marker, was maintained at a constant level or even increased during the 3D culture (Figure 2(d)).

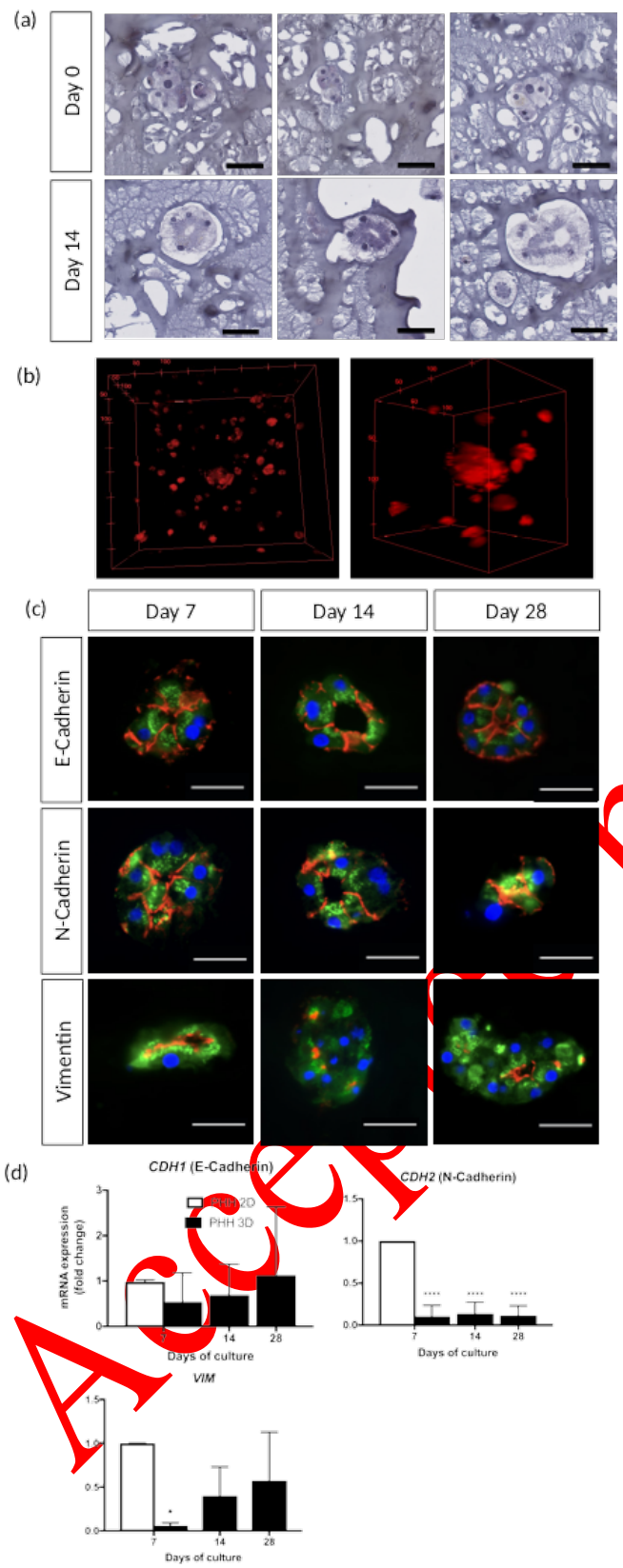

Figure 2 Phenotype of PHH 3D

(a) HE staining of PHH in 5% GelMa at 0 and 14 days of culture. Scale bar = 50 µm. (b) TPEF imaging and 3D reconstruction of PHH in GelMa at 14 days of culture. Scale bar units : µm (c) Immunofluorescence imaging of PHH spheroids with localization of E-Cadherin, N-Cadherin, or Vimentin (red) at days 7, 14 and 28 of culture. Green: Albumin; Blue: DAPI. Scale bar = 50 µm. (d) Expression of CDH1, CDH2 and VIM genes analyzed by qPCR in 3D PHH at days 7, 14 and 28 of culture, and in 2D PHH at day 7. Gene expression was normalized to that of the control (2D PPHs at day 7). Results shown are mean ± SD of n= 3 different donors.

3.2. PHH are maintained in a highly differentiated state in GelMa.

We performed 3' SRP-RNA-Seq data analyses to compare freshly isolated human hepatocyte (PHH T0) to 2D and 3D PHH primary cultures. The state of differentiation of PHH cultivated in 2D is at its peak on day 4 [3] and served as our 2D differentiation control. 3D PHH were analyzed at day 14 when the cells are well settled in spheroids in the GelMa. Compared to PHH T0, 51.42 % of up-regulated and 60.75 % of down-regulated genes were common between 2D and 3D PHH (Figure 3(a)). The GO-terms enrichment analysis showed that different regulatory processes/responses/pathways were specifically up-regulated in 3D PHH compared to freshly isolated cells whereas some were down regulated (Supplemental Figure 2). Up-regulated processes (cell substrate adhesion, integrin signaling, epithelial cell development, cell junction organization) were more related to cell-cell communications and interactions with the 3D matrix mainly reflecting the adaptation of cells to their new microenvironment, whereas down-regulated genes were associated with decreased acute inflammatory/immune responses and fatty acid metabolic processes. In comparison, the GO-terms associated with specifically up-regulated genes in 2D PHH compared to PHH T0 (platelet degranulation, response to tumor necrosis factor, humoral immune response, regulation of apoptotic signaling pathway, extrinsic apoptotic signaling pathway) were indicative of cellular reactions to environmental stress via immune and/or death pathways. Interestingly, similar pathways seem to be associated with GO terms (acute inflammatory response, humoral immune response, regulation of response to wounding) of downregulated genes in 3D PHH vs PHH T0.

In order to further understand the biological status of the cells, we examined the genes differentially expressed

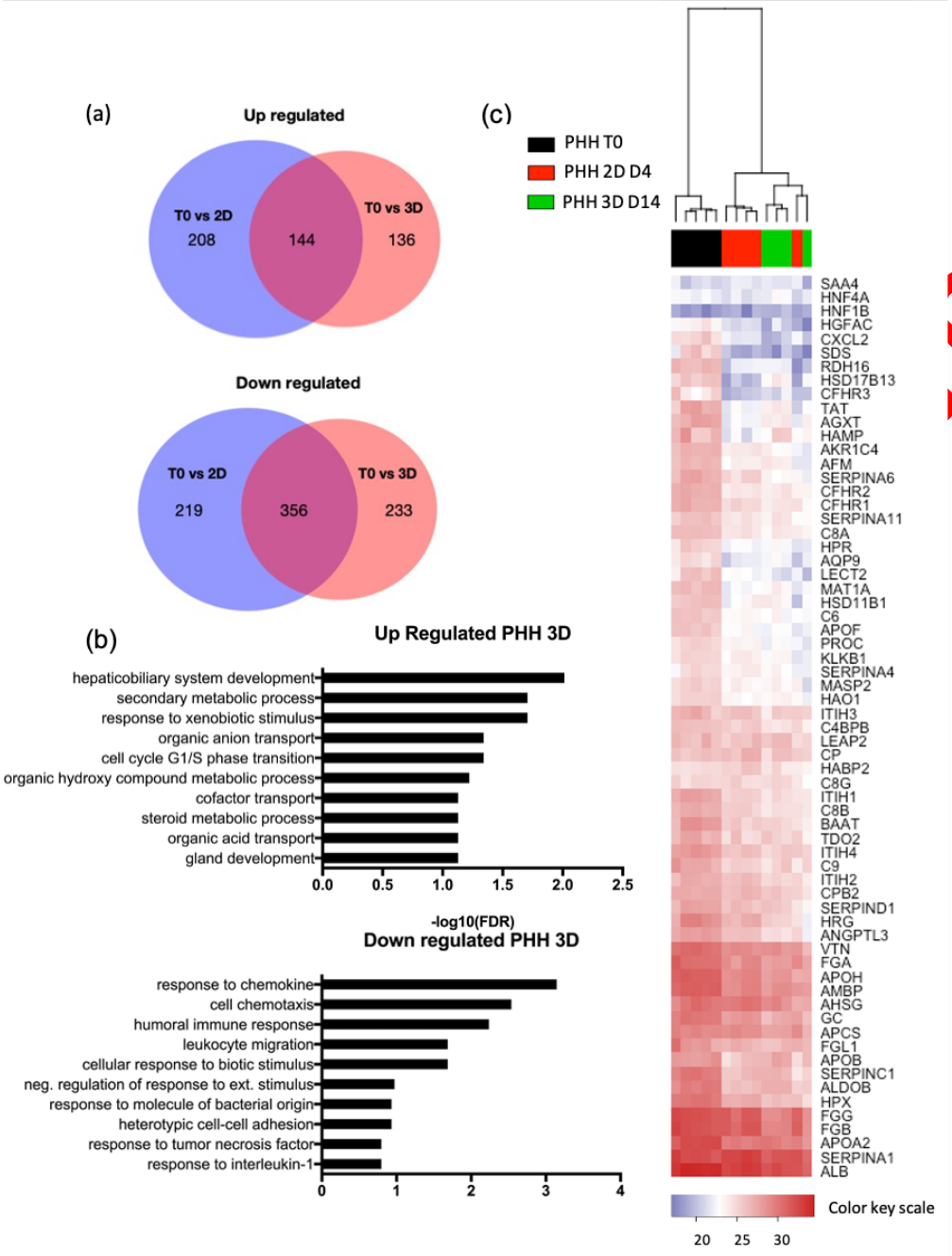

Figure 3 : Transcriptomic analysis of PHHs cultivated in 2D or 3D

(a) Venn diagram of Up and Down regulated genes in 2D PHHs at day 4 of culture and 3D PHHs at day 14, compared to freshly isolated PHH T0. (b) Gene set enrichment analysis based on the functional annotation of the Up and Down expressed genes in 3D PHHs compared to 2D PHHs. (c)Heatmap (-log2 z-scores) displaying the expression of LiGEP genes in freshly harvested PHHs (PHH T0, black, 5 samples), PHHs cultured in 2D for 4 days (red, 5 samples) or PHHs cultured in 3D in GelMa for 14 days (green, 4 samples). Samples and genes are hierarchically clustered based on Euclidian Distance according to their profile similarity. Elevated (red) and repressed (blue) expression are normalized to the mean of gene expression.

between 2D and 3D cultures. GO-terms enrichment analysis between these two cultures revealed that genes related to GO terms such as 'hepatobiliary system development', 'secondary metabolic process', 'response to xenobiotic stimulus', 'organic anion transport', 'cell cycle G1/S phase transition' (Figure 3(b)) were the most up-regulated in 3D PHH (between 1 to 2 log10 FDR (false discovery rate)) compared to 2D PHH. Other sets of genes related to response to chemokine, cell chemotaxis, immune response, external stimulus

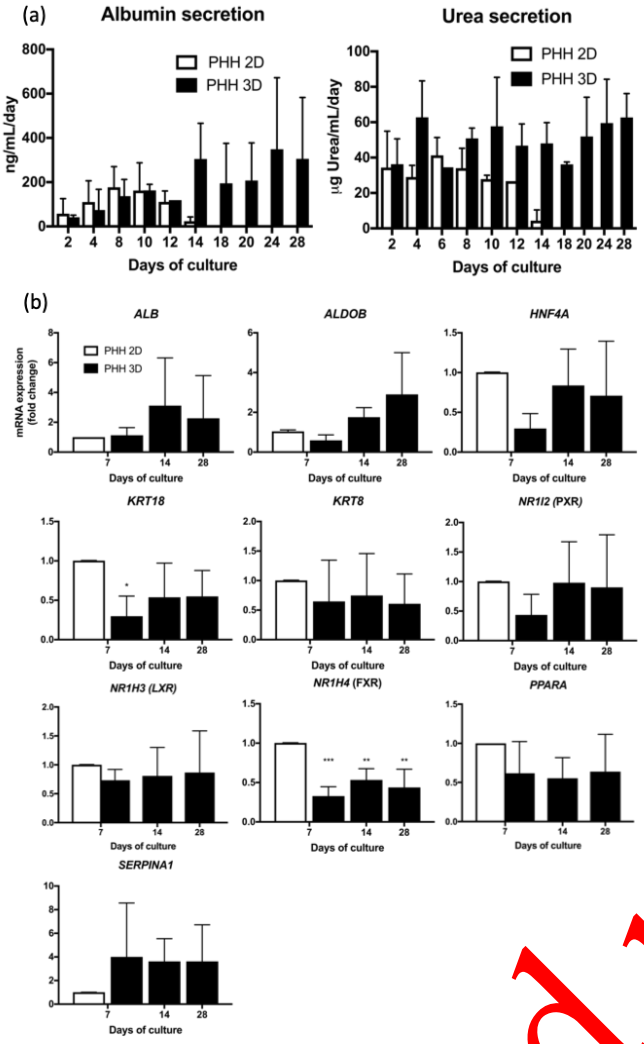

Figure 4: Hepatic differentiation of PHH cultured in GelMa for up to 28 days

(a) Albumin secretion (left) and urea secretion (right) of 3D PHH and 2D PHH over 28 days of culture. Results shown are mean SD of n= 4 different donors. (b) Expression of hepatic genes analyzed by qPCR 3D PHH at days 7, 14 and 28 of culture, and of 2D PHH at day 7. Gene expression was normalized to that of the control (2D PPHs at day 7). Results shown are mean ± SD of n=3 different donors.

response and cytokines were down-regulated in 3D PHH compared to 2D PHH, which suggests that PHH could be subjected to greater stress in 2D compared to 3D conditions.

We then analyzed the liver-specific gene expression (LiGEP) which was defined by Kim et al. (2017). This panel of genes is based on RNAs differentially expressed between liver and non-liver samples. The authors developed an algorithm to assess the differentiation or maturation status of samples with respect to 93 liver-specific genes validated using the Human Protein Atlas database and by quantitative real-time PCR [48]. LiGEP heat maps revealed a great homology of gene expression profiles between the 2D cultures on day 4 and the 3D cultures on day 14, showing good maintenance of many liver functions (Albumin, SerpinA1/C1, Aldolase B, APOA2/B/H, alpha1 Microglobulin, alpha2 Glycoprotein, Fibrinogen, Vitronectin, Amyloid P Component…) (Figure 3(c)) in 3D. Indeed, the LiGEP gene signature of 3D PHH in GelMa is remarkably similar to that of 3D PHH in collagen [9] (Supplemental Figure 2) demonstrating the very good differentiation of PHH in our bioprinting conditions.

3.3. Long term differentiation of 3D PHH in the presence or absence of FBS.

We then analyzed the long-term survival capacity of 3D PHH in GelMa by quantifying the secretion of two hepatic markers, albumin and urea. Unlike 2D PHH, in which secretions decrease considerably after day 10, 3D PHH are capable of expressing and secreting albumin and urea for at least 28 days of culture (Figure 4(a)). To confirm the long-term differentiation status of 3D PHH in GelMa, we then examined the expression of hepatic differentiation genes over 28 days (Figure 4(b)). Our results indicate that a panel of liver differentiation, receptors and transcription factors genes (*ALB, ALDOB, HNF4A, KRT18, KRT8, NR1I2, NR1H3, PPARA, SERPINA1*) were expressed and maintained in long-term 3D PHH cultures at levels equivalent or even higher than that found in 2D PHH cultures . We next examined the requirement of FBS in 3D PHH cultures. Indeed, the disadvantages of the presence of FBS in the culture could outweigh its benefits. Variations in the composition of the different FBS batches and the non-identification of certain constituents that could interact with the tested substances and could reduce the reproducibility of the assays. In addition, the utilization of FBS would be problematic for potential transient artificial liver support using hepatic bioreactors, which could introduce potential contaminations (viruses, prions...) and other artifacts [49]. First, we showed that 3D PHH, in the absence of FBS, were able to express and secrete albumin and urea for at least 28 days at the same levels as culture containing FBS (Supplemental Figure 4(a) and 4(b)). We also found that all the liver differentiation genes, receptors and transcription factors tested were expressed at the same levels in the absence of FBS (Supplemental Figure 4(c)). Further analyses, focusing on hepatic genes linked to phase I and phase II metabolism, and expression of hepatic transporters, confirmed the maintenance of differentiation in PHH cultured without FBS (Supplemental Figure 4(d)). In

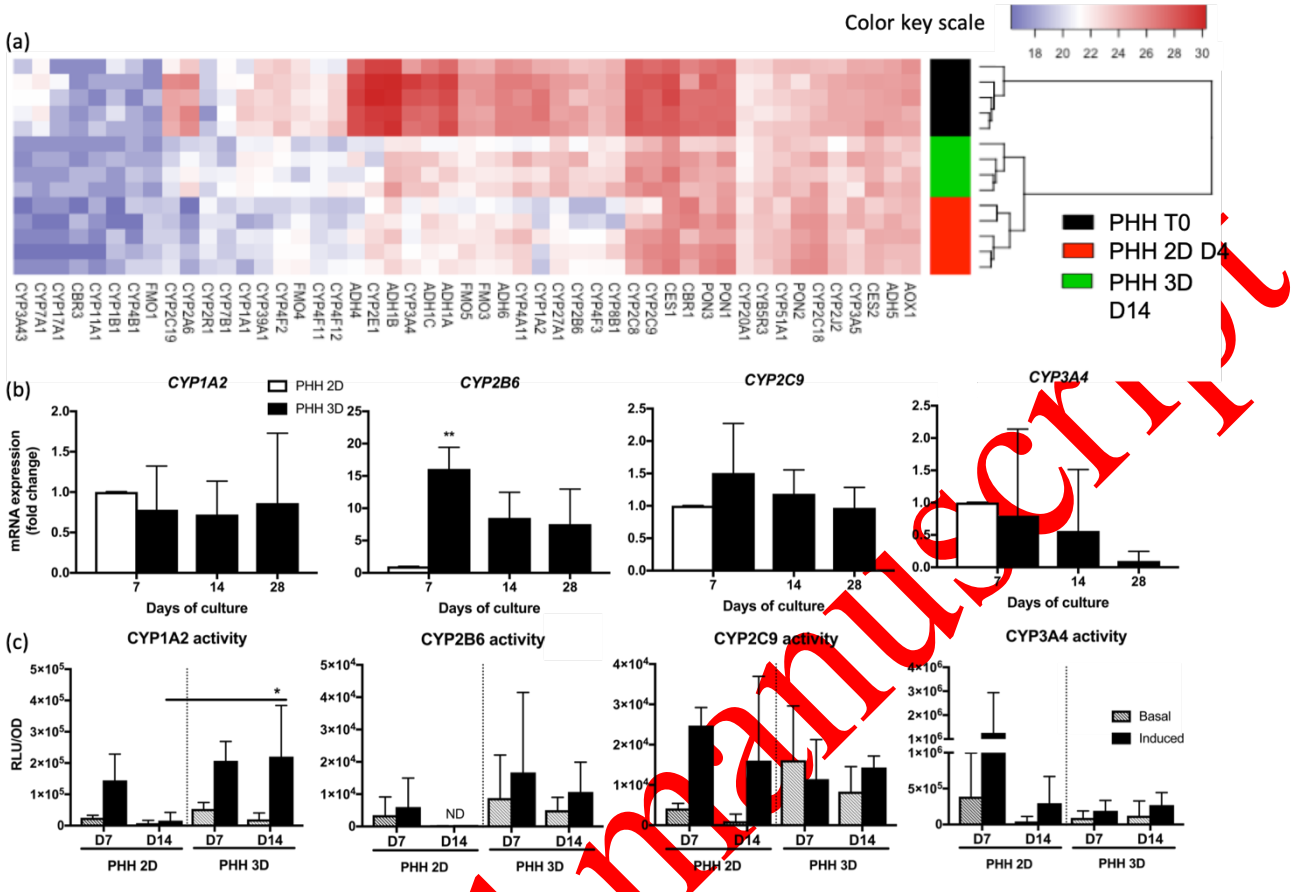

Figure 5 : Expression and activities of Phase I enzymes in 3D PHH

(a) Heatmap displaying the expression of Phase I enzyme genes (-log2 z-scores) in freshly isolated PHH (PHH T0, black, 5 samples), PHH cultured in 2D for 4 days (red, 5 samples) or PHH cultured in 3D for 14 days (green, 4 samples). Samples and genes are hierarchically clustered based on Euclidian Distance according to their profile similarity. Elevated (red) and repressed (blue) expression are normalized to the mean of gene expression. (b) Expression of CYP enzyme genes analyzed by qPCR in 3D PHH at days 7, 14 and 28 of culture, and 2D PHH at day 7. Gene expression was normalized to that of GAPDH and compared to that of the control (2D PHH at day 7). Results shown are mean ± SD of n=3 different donors. (c) CYP1A2, CYP2B6, CYP3A4 and CYP2C9 basal (hatched) and induced (black) activities of 2D and 3D PHH 3D assessed at day7 , and 14 of culture. ND: not detected. Results shown are mean ± SD of n=3 different donors.

addition, 3D cultures in GelMa could also be performed with cryopreserved PHH since the same expression levels of hepatic genes were measured in cultures from freshly isolated PHH and cryopreserved PHH (Supplemental Figure 5(a)).

3.4. Xenobiotics metabolism functions and proliferation capacities of 3D PHH .

To assess the expression of xenobiotics-metabolizing enzymes, we first examined heatmaps of the expression of phase I metabolism genes in 3D PHH compared to their expressions in freshly isolated PHH (PHH T0) and 2D culture at day 4 (2D PHH). Interestingly, the pattern of expression for drug-metabolizing enzymes genes in 3D PHH is closer to that of 2D PHH , rather than to the one of freshly isolated PHH, confirming that 3D PHH remain fully functional after two weeks of culture (Figure 5(a)).

CYPs are the major enzymes implicated in the phase I xenobiotic-metabolism pathway, playing a crucial role in the bioactivation of many drugs and contaminants. By RT-qPCR, we validated that for the major liver CYP genes, mRNA expressions were equal (*CYP1A2, CYP2C9, CYP3A4*) or higher (*CYP2B6*) in 3D PHH compared with 2D PHH (Figure 5(b)). These expression levels were maintained for at least 28 days confirming the high stability of 3D PHH. Interestingly, no difference could be observed between PHH in the presence or absence of FBS (Supplemental Figure 4(d)). Basal activities of all these CYPs (CYP1A2, CYP2B6,

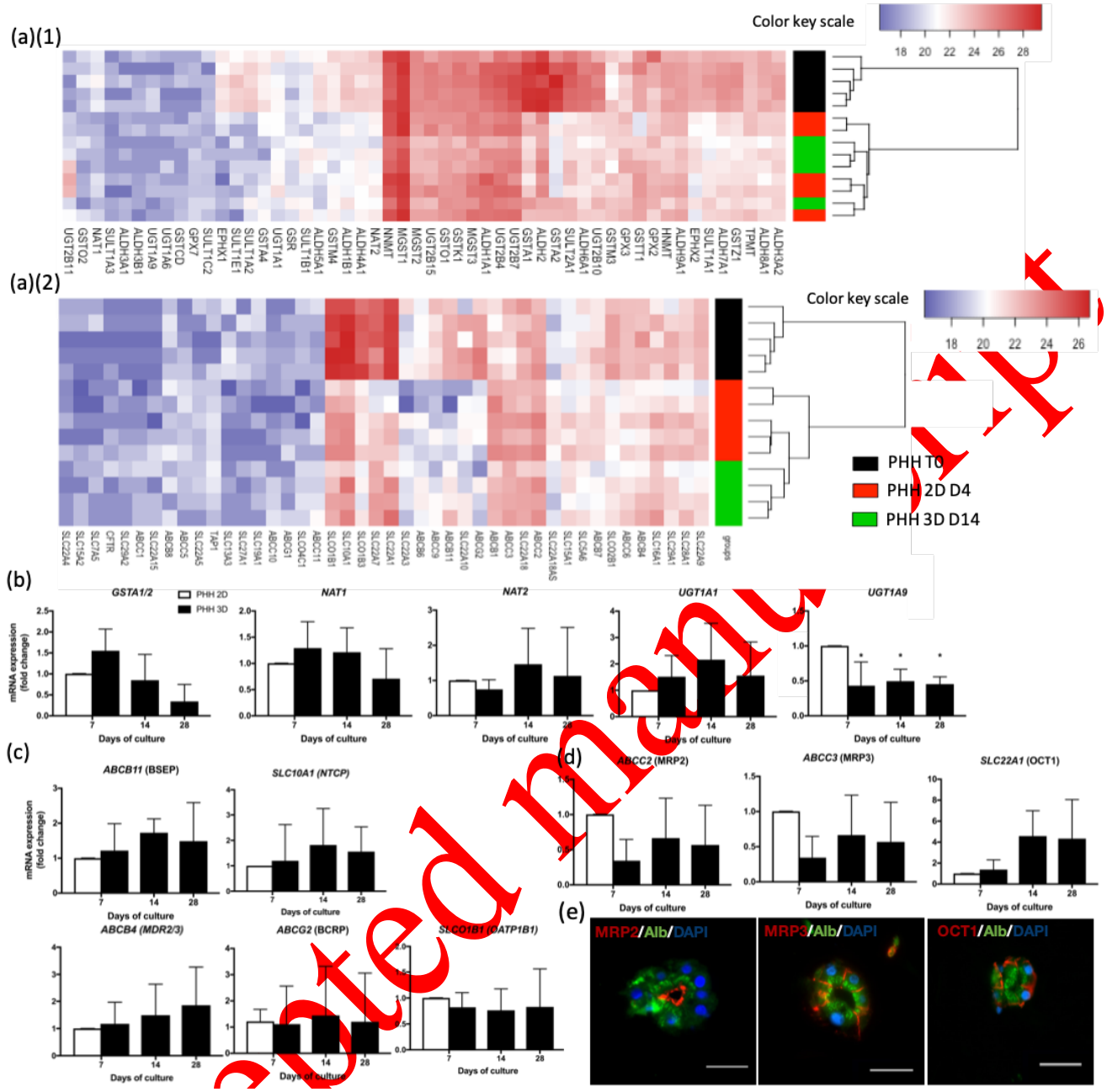

Figure 6 Expression of phase II enzymes in 3D PHH

(a) Heatmap (-log2 z-scores) displaying the expression of phase II enzyme genes (a)(1) and transporter genes (a)(2) in freshly isolated PHH (PHH T0, black, 5 samples), 2D PHH cultured for 4 days (red, 5 samples) or 3D PHH cultured for 14 days (green, 4 samples). Samples and genes are hierarchically clustered based on Euclidian Distance according to their profile similarity. Elevated (red) and repressed (blue) expression are normalized to the mean of gene expression.(b) Expression of phase II enzyme genes analyzed by qPCR in 3D PHH at days 7, 14 and 28 of culture, and 2D PHH at day 7. Gene expression was normalized to that of the control (2D PHH at day 7). Results shown are mean ± SD of n=3 different donors.(c) Expression of transporter genes analyzed by qPCR in 3D PHH at days 7, 14 and 28 of culture, and 2D PHH at day 7. Gene expressions were normalized to that of the control (2D PHH at day 7). (d) Expression of transporter genes analyzed by qPCR in 3D PHH at days 7, 14 and 28 of culture, and 2D PHH at day 7. Gene expression was normalized to that of the control (2D PPHs at day 7). Results shown are mean ± SD of n=3 different donors. (e) Immunofluorescence imaging of PHH spheroids with localization of MRP2, MRP3 and OCT1 (red) at day 14 of culture. (Green: Albumin; Blue: DAPI. Scale bar= 50 µm.) All results shown are mean ± SD of n=3 different donors.

CYP2C9, CYP3A4) could be measured at 7 and 14 days in 3D PHH (Figure 5(b)). CYP1A2, CYP2B6 and CYP3A4 activities could be induced in 3D cultures at the same or higher levels than in 2D culture (Figure 5(c)) whereas CYP2C9 activities/inductions in PHH 3D were lower but with higher basal activity. Basal and induced CYP1A and CYP1A2 could be measured, respectively, by EROD and MROD activity measurement [50] after

28 days of culture, showing that chronic and long-term effects of drugs and environmental contaminants could be tested in this 3D PHH model (Data not shown).

We then compared the mRNA expression of phase II metabolism enzymes and hepatic transporters, and found for the most part equivalent levels in 3D PHH and 2D PHH (Figure 6(a.1) and 6(a.2)). By RT-qPCR, we confirmed that the expression of phase II xenobiotic metabolism enzymes (*GSTA1/2, NAT1, NAT2, UGT1A1, UGT1A9*) and transporters (*ABCB11, ABCG2, SLC10A1, ABCB4, SLCO1B1, ABCC2, ABCC3, SLC22A1*) were stably expressed in 3D PHH up to 28 days of culture (Figure 6(b) and 6(c)). *ABCC3* (MRP3) and *SLCO1B1* (OCT1) were also expressed at the same or higher level in 3D PHH compared to 2D PHH (Figure 6(d)) and the hollow spheroid organization was concomitant with the polarization of PHH. MRP2 was located exclusively at apico/canicular zones while MRP3 and OCT1 were expressed at intercellular junctions confirming the polarization of PHH clusters throughout the time in culture (Figure 6(e)).

We recently described for the first time that 3D PHH in collagen gel can proliferate *in vitro* [9]. Since the two models, 3D PHH in collagen and 3D PHH in GelMa, display strong similarities in morphology, polarity, differentiation and biotransformation capacities, we examined the possibility of 3D PHH in GelMa to proliferate. We quantified immunolocalized cyclin D1 (Figure 7(a)) and the incorporation of EdU (Figure 7(b)) in spheroids as indicators of progression in late phase G1 and DNA replication, respectively. Albumin was used as a positive control to confirm the identity of PHH. Our results demonstrated the proliferation of 3D PHH in GelMa throughout the time in culture, as shown by the high proportion cyclin positive nuclei and EdU+/Alb+ cells between days 4-6 and day 28. An optimum was reached at day 10-12 with approximately 40 % and 30 % of cells positive for cyclin D1 and EdU, respectively. 3D PHH cultures using PHH from four different donors gave similar results with only slight variations in the kinetic of CyD1+/Alb+ and EdU+/Alb+ expression whereas in 2D PHH cultures were always cyclin D1 and EdU negatives (data not shown).

3.5. Transplantation of 3D PHH in mice

In addition to being a well-suited matrix for three-dimensional extrusion bioprinting to generate functional and proliferative *in vitro* models of hepatic cells, GelMa

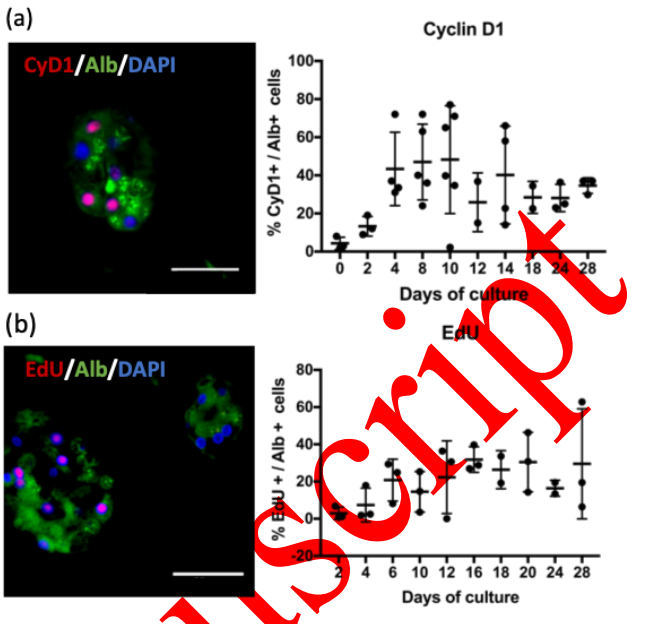

Figure 7 : 3D PHH proliferate for at least 28 days in culture.

(a) Representative staining (left) and time course (right) of the proliferation marker Cyclin D1 in 3D PHH at different time points of culture. Green = albumin, Red= Cyclin D1, scale bar = 50 µm. (b) Representative staining (left) and time course (right) of the incorporation of the thymidine analogue EdU, an index of DNA replication, in 3D PHH at different time points of culture. Green = albumin, red = EdU, scale bar = 50 µm. For each time point, mean ± SD of at least n=3 different donors is shown

has also been described as biocompatible for implantation in animal hosts [51], [52]. We therefore assessed the feasibility and the potential of *in vivo* transplantation of our 3D models. We bioprinted 3D PHH structures using 3 different PHH donors. The bioprinted model displays large channels increasing the exchange surface between matrix and external environment, thus improving solute/gas exchanges. Structures were cultivated 7 days in 3D, before being subcutaneously implanted in NSG mice (Figure 8(a)). After 28 days post-implantation, the structures were retrieved and the autofluorescence of viable cells was observed by TPEF (Figure 8(b)). The results showed a large number of auto fluorescent cells, which was accompanied by detection of human albumin in the serum of the transplanted mice confirming the presence of functional hepatocytes. In mice transplanted with the sham structures no cells were seen by TPEF and no albumin could be detected (data not shown). To analyze the functionality of 3D PHH engrafted *in vivo*, we also analyzed the implanted structures for the presence of

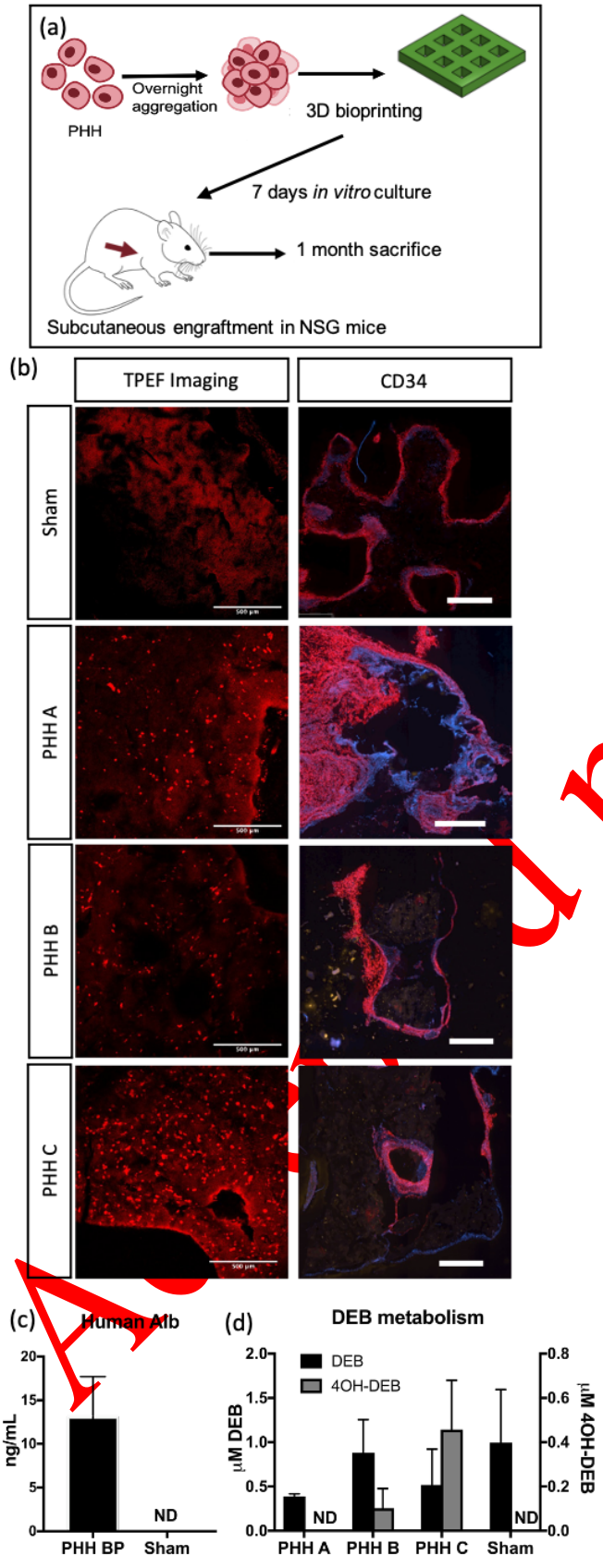

Figure 8 : Engraftment of 3D printed structures in a mouse model

(a) Diagram summarizing the experimental steps in generating 3D PHH and their implantation in host mice. 3 lots of cryopreserved PHH (see Supplemental) and a Sham control were printed and implanted in triplicates. (b) Left panel: TPEF imaging of the sham or hepatocytes loaded structures (3 different donors) recovered 28 days post engraftment. Scale bar = 500 µm. Right panel: Immunofluorescence imaging of the structures with localization of CD34 (red) at day 14 of culture. Blue: DAPI. Scale bar= 1 mm. (c) Measurement of human albumin by ELISA in the serum of the mice at 28 days. No albumin was detected (ND) in mice implanted with sham structures. Results shown are mean ± SD, n=3 for each condition. (d) Dosage of DEB and 4OH-DEB in mice serum at 28 days post engraftment. Results shown are mean ± SD, n=3 for each condition.

immature endothelial cells (CD34 positive cells) that might indicate their neovascularization. A high number of CD34- positive cells could be observed around the gel and in the channels indicative of the neovascularization of the reimplanted structures (Figure 8(b)).

The neovascularization of the structures was also corroborated by the presence of human albumin in the serum of transplanted mice (Figure 8(c)). In addition, transplanted 3D PHH were able to metabolize debrisoquine (DEB), which is catalyzed by human CYP2D6 and is not metabolized in mice. After treatment with debrisoquine, 4-hydroxydebrisoquine (4OH-DEB) was detected in the serum of transplanted mice (Figure 8(d)). 4OH-DEB could not be detected in the serum of control mice in which the presence of DEB was confirmed. Our study shows that, in parallel to a gradual establishment of vascularization, 3D PHH established in GelMa can be maintained in a differentiated state at least 28 days after transplantation into mice.

4. Discussion

Over these last years, 3D cultures in matrix with various stiffness have been developed to more closely mimic cell behavior *in vivo* than 2D cultured cells [9], [13]–[15], [17]. In matrix-based models of embedded transformed hepatic cells, increasing matrix stiffness has been shown to promote the development of spheroids with increasing biotransformation activities; showing that 3D matrices are an attractive tool for studying rigidity-dependent homeostasis [17]. In very recent studies, we have defined optimal conditions for the proliferation of adult human hepatocytes in 3D collagen following a rapid (12h) pre-aggregation of cells before their inclusion in the collagen matrix. This model allowed us to

demonstrate the ability of cells to undergo at least two waves of proliferation after incorporation into the matrix [9].

Our aim was to combine those 3D models of proliferative, differentiated PHH with the bioprinting technology to obtain reproductible functional human organoids with high liver functions, long-term survival and transplantation potential. The bioprinting process can be used to obtain complex, controlled architectures of the structure, that more closely resemble the architecture of native tissues, thus optimizing their transplantation potential in mice, as well as their incorporation in microfluidic devices compared to classical 3D matrix culture. In this work, we used an extrusion-based system to print PHH in a methacrylated gelatin matrix and named the resulting cell model Hepoid in GelMa.

Due to its poor mechanical properties and its lack of post-bioprinting polymerization capacity, collagen is not an optimal matrix for bioprinting. On the other hand, GelMa is a hydrogel compatible with a wide range of bioprinting systems, and its utilization in extrusion based bioprinting has been largely documented [42], [43]. Because both of its natural (gelatin) and synthetics (methacrylation) origins, GelMa ensures good cell viability while ensuring the maintenance of the printed structures throughout extended time in culture. Bioprinting of transformed hepatocytes [25], [30], [31] or induced pluripotent cells [28] have proven their ability for optimal cell line differentiation. Recently that we have shown that, by using low concentrations (5%) of GelMa and photoinitiator, and by recreating, before bioprinting, intercellular contacts, we got the possibility of differentiating and maintaining over a long time bioprinted hepatic cells lines [25]. The very high viability of PHH over a long period is here enabled by the use of low concentration of GelMa and photo-initiator. 5% GelMa is highly porous, thus ensuring excellent physical diffusion of oxygen and biological molecules across up to 3 mm deep [53]. While providing a suitable microenvironment for the long term viability of the cells, the selected parameters for bio-ink and photo-initiator also ensure the structural integrity of the printed models throughout the 28 days of culture [25].

The need to establish, prior to bioprinting, intercellular contacts for optimal survival and maintenance of hepatic functions has been confirmed by the approaches adopted by Organovo [27], [41] and Cyfuse Biomaterials [39], [40], the only two companies to have currently succeeded in bioprinting PHH. Using our technique, light cellular interactions are created by forming small aggregates of cells in ULAP over a short period (12 hours), prior to gel incorporation. This also avoids the classic problem of formation of necrotic centers due to hypoxia in large size spheroids [54].

Intercellular junctions between hepatocytes are key to the maintenance of the hepatic phenotype and functionality (secretion of albumin, production of urea, glycogenolysis, phase I metabolism and biliary secretion) [36], [55]–[57]. In our Hepoid in GelMa model, the initial presence of these cellular contacts favors the organization into polarized and differentiated spheroids. It is notably characterized by the progressive increase in expression and appropriate intracellular localization of E-cadherin, a key protein for differentiation, polarization and regulation of hepatic functions [22], [58]. Intercellular junctions also favor the polarization of the spheroid cells, as demonstrated by the specific localization of the MRP2 transporter at the apical pole and of the MRP3 and OCT1 transporters at the intercellular junctions, thus recreating a biliary pole located toward the lumen of the spheroids. This organization of a monolayer of polarized cells around a lumen in the spheroids, is a unique feature of our 3D model. So far, other PHHs spheroids obtained did not show any specific organization: the bile canaliculi, if present, are located diffusely and the polarization and transport markers are heterogeneously expressed inside the spheroids. [6]–[8]. Thus, 3D PHHs, whether in collagen or in GelMa, have a key advantage in the evaluation of the transport activities of both endogenous and exogenous molecules.

Throughout the 28 days of culture, Hepoid in GelMa display features of differentiated hepatocytes with upregulation of the hepatobiliary functions and metabolic processes exemplified by the secretion of albumin and urea. Most hepatic markers and phase I, II and III detoxification enzymes can be maintained for at least 28 days at a level well above conventional short-time 2D culture conditions. In addition, the absence of FBS in the medium does not interfere with cell viability, differentiation, and detoxification enzyme levels which is a valuable feature for many applications in toxicology, biotechnology and the development of bioreactors [49].

In the liver, hepatocytes are quiescent, non-proliferative cells. Upon liver damage due to partial hepatectomy or drug mediated acute toxicity, hepatocytes are able to initiate a regeneration process by entering a proliferative

stage [49]. When isolated and cultured *in vitro*, human hepatocytes lose these proliferative abilities and quickly enter apoptosis. *In vitro* proliferation of PHH thus remains one of the key challenges to generate hepatic models for the development of organoids, or for prediction of toxicity or genotoxicity. Our results show that Hepoid in GelMa can proliferate throughout the culture time, with stable and maximum proliferation 4 days after bioprinting. We previously demonstrated that 3D PHH are able to proliferate when precise conditions of cell–cell interactions and appropriate collagen concentration/rigidity are met [9]. Proliferation in GelMa appeared to be reduced compared to collagen conditions [9], indicating that matrix structure and rigidity are important determinants of hepatocyte proliferation [16], [20], [25], [59].

The generation of stable transplantable PHH structures for future transient hepatic assistance or drug research remains a long-term goal. The first results of implantation of bioprinted hepatic structures were obtained by Zhong et al., with collagen/chitosan 3D printed structures loaded with the L-02 cell line [33]. More recently, using 3D bioprinted HepaRG cells in alginate/gelatin, Yang et al reported data showing that HepaRG could have *in vivo* hepatic functions and alleviated liver failure after transplantation in mice [34]. In addition, transplantation of induced hepatocytes-like cells in an *in vivo* environment, with complex chemical signaling, suggested promotion of hepatocyte differentiation [60]. The high and stable viability of Hepoid in GelMa allowed us to perform long term PHH implantations in mice. GelMa has long been shown to be a suitable matrix for engraftment. Due to its natural origin, it possesses RGD-motif sites, which promote post-implantation proteolytic degradation by collagenases. The RGD sites are also crucial for promoting the adherence of endothelial cells and the vascularization [26], [52]. In our model, the GelMa-based bioprinted structures remain stable and are easily recovered 28 days post engraftment. PHH remain differentiated and their vascularization promotes their normal hepatic functions as evidenced by the detection of human albumin and of human CYP2D6-specific 4OH-DEB in the serum of the mice. Immature CD34-positive endothelial cells, around the structure and inside the bioprinted channels, confirm neovascularization of the implanted structures. Results obtained for the DEB metabolism showed variations between the three different donors, mainly due to the maintenance, post-transplantation, of existing interindividual differences in the kinetics of CYP2D6-mediated metabolism and DEB/metabolites distribution. Those differences between DEB and 4OH-DEB may be explained by different CYP2D6 metabolic kinetics, phase II metabolism enzymes, or 4OH-DEB elimination. These initial results demonstrate the technical feasibility of replantation in mice, the main obstacle being the quantity of cells to be obtained (40 to 60 million) for efficient transient rescue. We are considering here the resolution of this technical lock by printing higher cell densities (up to 40×10^6/mL) and transplanting several structures in the same animal.

3D bioprinting of hepatic cells is very promising for tissue engineering, as it provides a suitable environment for cell differentiation and growth while allowing the production of structures with complex architecture. In addition to the beforementioned *in vivo* therapeutic delivery systems or future transient liver rescues, 3D bioprinting of Hepoid in GelMa is particularly relevant for *in vitro* applications in physiopathology studies or its adaptation to microfluidic techniques. The coupling of 3D cultured cells to a perfusion device contributes to oxygen delivery, improves cell survival and is important for mid/long-term culture of functional oxygenated bioreactors.

Perfusion-based systems of HepG2 or HepaRG cells have been successfully bioprinted into decellularized liver matrix/GelMa or GelMa, indicating this matrix suitability for microfluidic/bioreactor developments of hepatic cells [29], [30], [61], [62]. The chips that have been developed so far are composed of cells from lines derived from hepatocarcinomas [29], [30], [32], [63], utilization of HHP with those technologies would allow an exhaustive evaluation of the metabolic mechanisms taking place in the liver micro-environment. In addition, an issue that is increasingly discussed is the addition of hepatic non-parenchymal cells, whose importance in the functionality of hepatocytes and response to stimuli has been widely highlighted [62], [64], [65]. For example, the bioprinting of HepaRG cells with stellate and/or endothelial cells might potentially be used to study the development of hepatic pathologies (i.e liver fibrosis), due to the action of cells-cells interaction on the synthesis and deposition of collagen fibrils [25].

Thus, the next step will be to combine the capacity of bioprinting to recreate complex three dimensional structures with controlled and spatially differentiated deposits of different hepatic cell types. Then, coupling these bioprinted multicellular microchips with microfluidic perfusion systems will make it possible to

generate perfusable cells/matrix organizations. This will enable us to control shear flows, scalable mechanical forces as well as oxygenation and delivery of growth factors/cytokines to hepatocytes embedded in the matrix. This will provide powerful tools to faithfully model pathophysiological conditions and for applications in biotechnological developments and drug screening.

Acknowledgements

The authors thank the platforms from the SFR Biosit (UMS CNRS 3480 / US INSERM 018, Biogenouest, University of Rennes 1): MRic-Photonics, MRic-Biphoton, BiM-3D, H2P2, CRB Santé of Rennes. This work was supported by France Relance, the Institut National de la Santé et de la Recherche Médicale (Inserm), the University of Rennes 1, the Ligue Contre le Cancer du Grand Ouest, the Institut National du Cancer (INCa) . MC has been a recipient of a fellowship from Inserm, the INCa (#2018-142) and the Région Bretagne. The authors also wish to thank Dr. Catherine Lavau for her careful proofreading of the article.

Author's contributions:

MC: Investigation, Writing – original draft / review & editing; SR: Methodology, Resources; FE: Investigation; UJ: Investigation, Resources; HO: Resources; AB: Investigation; CD: Resources, Supervision; VL: Formal analysis; SL: Conceptualization, Supervision, Writing – review & editing; GB: Conceptualization, Funding acquisition, Writing – original draft / review & editing

Data availability statement

The authors declare that all data supporting the results of this study are available within the paper and in Supplementary Information, and are also available from the corresponding author upon reasonable request.

Ethical statement

All animal procedures were performed according to institutional guidelines (Agreement APAFIS # 7163; regional ethics committee of Brittany; France).

References

[1] L. A. Stanley, "Drug Metabolism," in *Pharmacognosy*, Elsevier, 2017, pp. 527–545. Accessed: Jul. 20, 2019. [Online]. Available: https://doi.org/10.1016/B978-0-12-802104-0.00027-5

[2] E. L. LeCluyse, P. L. Bullock, and A. Parkinson, "Strategies for restoration and maintenance of normal hepatic structure and function in long-term cultures of rat hepatocytes," *Advanced Drug Delivery Reviews*, vol. 22, no. 1, pp. 133–186, 1996, doi: https://doi.org/10.1016/S0169-409X(96)00418-8.

[3] G. Elaut *et al.*, "Molecular Mechanisms Underlying the Dedifferentiation Process of Isolated Hepatocytes and Their Cultures," *Current Drug Metabolism*, vol. 7, no. 6, pp. 629–660, Aug. 2006, doi: 10.2174/138920006778017759.

[4] A. Guillouzo, F. Morel, O. Fardel, and B. Meunier, "Use of human hepatocyte cultures for drug metabolism studies," *Toxicology*, vol. 82, no. 1, pp. 209–219, 1993, doi: https://doi.org/10.1016/0300-483X(93)90065-Z.

[5] H. Olson *et al.*, "Concordance of the Toxicity of Pharmaceuticals in Humans and in Animals," *Regulatory Toxicology and Pharmacology*, vol. 32, no. 1, pp. 56–67, Aug. 2000, doi: 10.1006/rtph.2000.1399.

[6] S. Messner, I. Agarkova, W. Moritz, and J. M. Kelm, "Multi-cell type human liver microtissues for hepatotoxicity testing," *Archives of toxicology*, vol. 87, no. 1, pp. 209–213, 2013, doi: https://doi.org/10.1007/s00204-012-0968-2.

[7] D. F. G. Hendriks, L. Fredriksson Puigvert, S. Messner, W. Mortiz, and M. Ingelman-Sundberg, "Hepatic 3D spheroid models for the detection and study of compounds with cholestatic liability," *Scientific reports*, vol. 6, pp. 35434–35434, 2016, doi: https://doi.org/10.1038/srep35434.

[8] C. C. Bell *et al.*, "Characterization of primary human hepatocyte spheroids as a model system for drug-induced liver injury, liver function and disease," *Scientific Reports*, vol. 6, no. 1, p. 25187, Jul. 2016, doi: 10.1038/srep25187.

[9] S. Rose *et al.*, "Generation of proliferating human adult hepatocytes using optimized 3D culture conditions," *Sci Rep*, vol. 11, no. 1, p. 515, Dec. 2021, doi: 10.1038/s41598-020-80019-4.

[10] K. P. Kanebratt *et al.*, "Primary Human Hepatocyte Spheroid Model as a 3D In Vitro Platform for Metabolism Studies," *Journal of Pharmaceutical Sciences*, vol. 110, no. 1, pp. 422–431, Jan. 2021, doi: 10.1016/j.xphs.2020.10.043.

[11] S. U. Vorrink, Y. Zhou, M. Ingelman-Sundberg, and V. M. Lauschke, "Prediction of Drug-Induced Hepatotoxicity Using Long-Term Stable Primary Hepatic 3D Spheroid Cultures in Chemically Defined Conditions," *Toxicological Sciences*, vol. 163, no. 2, pp. 655–665, Jun. 2018, doi: 10.1093/toxsci/kfy058.

[12] W. R. Proctor *et al.*, "Utility of spherical human liver microtissues for prediction of clinical drug-induced liver injury," *Archives of toxicology*, vol. 91, no. 8, pp. 2849–2863, 2017, doi: 10.1007/s00204-017-2002-1.

[13] R. Glicklis, L. Shapiro, R. Agbaria, J. C. Merchuk, and S. Cohen, "Hepatocyte behavior within three-dimensional porous alginate scaffolds," *Biotechnology and*

Bioengineering, vol. 67, no. 3, pp. 344–353, 2000, doi: 10.1002/(SICI)1097-0290(20000205)67:3<344::AID-BIT11>3.0.CO;2-2.
[14] S. C. Ramaiahgari *et al.*, "A 3D in vitro model of differentiated HepG2 cell spheroids with improved liver-like properties for repeated dose high-throughput toxicity studies," *Archives of Toxicology*, vol. 88, no. 5, pp. 1083–1095, 2014, doi: 10.1007/s00204-014-1215-9.
[15] A. Takai *et al.*, "Three-dimensional Organotypic Culture Models of Human Hepatocellular Carcinoma," *Scientific Reports*, vol. 6, p. 21174, 2016, doi: https://doi.org/10.1038/srep21174.
[16] H. Hu *et al.*, "Long-Term Expansion of Functional Mouse and Human Hepatocytes as 3D Organoids," *Cell*, vol. 175, no. 6, pp. 1591–1606, Nov. 2018, doi: 10.1016/j.cell.2018.11.013.
[17] J. Bomo *et al.*, "Increasing 3D Matrix Rigidity Strengthens Proliferation and Spheroid Development of Human Liver Cells in a Constant Growth Factor Environment," *J. Cell. Biochem.*, vol. 117, no. 3, pp. 708–720, Mar. 2016, doi: 10.1002/jcb.25356.
[18] E. L. LeCluyse, K. L. Audus, and J. H. Hochman, "Formation of extensive canalicular networks by rat hepatocytes cultured in collagen-sandwich configuration," *American Journal of Physiology-Cell Physiology*, vol. 266, no. 6, pp. C1764–C1774, 1994, doi: 10.1152/ajpcell.1994.266.6.C1764. PMID: 8023906.
[19] R. Xu, A. Boudreau, and M. J. Bissell, "Tissue architecture and function: dynamic reciprocity via extra- and intra-cellular matrices," *Cancer Metastasis Rev*, vol. 28, no. 1–2, pp. 167–176, Jun. 2009, doi: 10.1007/s10555-008-9178-z.
[20] J. Schrader *et al.*, "Matrix Stiffness Modulates Proliferation, Chemotherapeutic Response and Dormancy in Hepatocellular Carcinoma Cells," *Hepatology (Baltimore, Md.)*, vol. 53, no. 4, pp. 1192–1205, Apr. 2011, doi: 10.1002/hep.24108.
[21] E. J. Semler, C. S. Ranucci, and P. V. Moghe, "Mechanochemical manipulation of hepatocyte aggregation can selectively induce or repress liver-specific function," *Biotechnology and Bioengineering*, vol. 69, no. 4, pp. 359–369, 2000, doi: 10.1002/1097-0290(20000820)69:4<359::AID-BIT2>3.0.CO;2-Q.
[22] M. Vinken *et al.*, "Involvement of Cell Junctions in Hepatocyte Culture Functionality," *Critical Reviews in Toxicology*, vol. 36, no. 4, pp. 299–318, Jan. 2006, doi: 10.1080/10408440600599273.
[23] D. MacPherson, Y. Bram, J. Park, and R. E. Schwartz, "Peptide-based scaffolds for the culture and maintenance of primary human hepatocytes," *Sci Rep*, vol. 11, no. 1, p. 6772, Dec. 2021, doi: 10.1038/s41598-021-86016-5.
[24] K. Bhadriraju and L. K. Hansen, "Hepatocyte adhesion, growth and di!erentiated function on RGD-containing proteins," p. 6, 2000.
[25] M. Cuvellier *et al.*, "3D culture of HepaRG cells in GelMa and its application to bioprinting of a multicellular hepatic model," *Biomaterials*, vol. 269, p. 120611, Feb. 2021, doi: 10.1016/j.biomaterials.2020.120611.
[26] D. B. Kolesky, R. L. Truby, A. S. Gladman, T. A. Busbee, K. A. Homan, and J. A. Lewis, "3D Bioprinting of Vascularized, Heterogeneous Cell-Laden Tissue Constructs," *Advanced Materials*, vol. 26, no. 19, pp. 3124–3130, May 2014, doi: 10.1002/adma.201305506.
[27] L. M. Norona, D. G. Nguyen, D. A. Gerber, S. C. Presnell, and E. L. LeCluyse, "Modeling compound-induced fibrogenesis in vitro using three-dimensional bioprinted human liver tissues," *Toxicological Sciences*, vol. 154, no. 2, pp. 354–367, 2016, doi: 10.1093/toxsci/kfw169.
[28] X. Ma *et al.*, "Deterministically patterned biomimetic human iPSC-derived hepatic model via rapid 3D bioprinting," *Proceedings of the National Academy of Sciences*, vol. 113, no. 8, pp. 2206–2211, Feb. 2016, doi: 10.1073/pnas.1524510113.
[29] N. S. Bhise *et al.*, "A liver-on-a-chip platform with bioprinted hepatic spheroids," *Biofabrication*, vol. 8, no. 1, p. 014101, Jan. 2016, doi: 10.1088/1758-5090/8/1/014101.
[30] T. Grix *et al.*, "Bioprinting Perfusion-Enabled Liver Equivalents for Advanced Organ-on-a-Chip Applications," *Genes*, vol. 9, no. 4, p. 176, Mar. 2018, doi: 10.3390/genes9040176.
[31] T. Hiller *et al.*, "Generation of a 3D Liver Model Comprising Human Extracellular Matrix in an Alginate/Gelatin-Based Bioink by Extrusion Bioprinting for Infection and Transduction Studies," *International Journal of Molecular Sciences*, vol. 19, no. 10, p. 3129, Oct. 2018, doi: 10.3390/ijms19103129.
[32] H. Lee *et al.*, "Cell-printed 3D liver-on-a-chip possessing a liver microenvironment and biliary system," *Biofabrication*, vol. 11, no. 2, p. 025001, Jan. 2019, doi: 10.1088/1758-5090/aaf9fa.
[33] C. Zhong, H.-Y. Xie, L. Zhou, X. Xu, and S.-S. Zheng, "Human hepatocytes loaded in 3D bioprinting generate mini-liver," *Hepatobiliary & Pancreatic Diseases International*, vol. 15, no. 5, pp. 512–518, Oct. 2016, doi: 10.1016/S1499-3872(16)60119-4.
[34] H. Yang *et al.*, "Three-dimensional bioprinted hepatorganoids prolong survival of mice with liver failure," *Gut*, vol. 70, no. 3, pp. 567–574, 2021, doi: 10.1136/gutjnl-2019-319960.
[35] A. Faulkner-Jones *et al.*, "Bioprinting of human pluripotent stem cells and their directed differentiation into hepatocyte-like cells for the generation of mini-livers in 3D," *Biofabrication*, vol. 7, no. 4, p. 044102, Oct. 2015, doi: 10.1088/1758-5090/7/4/044102.
[36] E. Goulart *et al.*, "3D bioprinting of liver spheroids derived from human induced pluripotent stem cells sustain liver function and viability *in vitro*," *Biofabrication*, vol. 12, no. 1, p. 015010, Nov. 2019, doi: 10.1088/1758-5090/ab4a30.
[37] Y. Kim *et al.*, "Three-dimensional (3D) printing of mouse primary hepatocytes to generate 3D hepatic structure," *Ann Surg Treat Res*, vol. 92, no. 2, p. 67, 2017, doi: 10.4174/astr.2017.92.2.67.

[38] A. Messina *et al.*, "Evidence of Adult Features and Functions of Hepatocytes Differentiated from Human Induced Pluripotent Stem Cells and Self-Organized as Organoids," *Cells*, vol. 11, no. 3, p. 537, Feb. 2022, doi: 10.3390/cells11030537.
[39] H. Kizawa, E. Nagao, M. Shimamura, G. Zhang, and H. Torii, "Scaffold-free 3D bio-printed human liver tissue stably maintains metabolic functions useful for drug discovery," *Biochemistry and Biophysics Reports*, vol. 10, pp. 186–191, Jul. 2017, doi: 10.1016/j.bbrep.2017.04.004.
[40] I. Ide, E. Nagao, S. Kajiyama, and N. Mizoguchi, "A novel evaluation method for determining drug-induced hepatotoxicity using 3D bio-printed human liver tissue," *Toxicology Mechanisms and Methods*, pp. 1–8, Nov. 2019, doi: 10.1080/15376516.2019.1686795.
[41] D. G. Nguyen *et al.*, "Bioprinted 3D Primary Liver Tissues Allow Assessment of Organ-Level Response to Clinical Drug Induced Toxicity In Vitro," *PLoS ONE*, vol. 11, no. 7, p. e0158674, 2016, doi: 10.1371/journal.pone.0158674.
[42] T. Billiet, E. Gevaert, T. De Schryver, M. Cornelissen, and P. Dubruel, "The 3D printing of gelatin methacrylamide cell-laden tissue-engineered constructs with high cell viability," *Biomaterials*, vol. 35, no. 1, pp. 49–62, Jan. 2014, doi: 10.1016/j.biomaterials.2013.09.078.
[43] L. E. Bertassoni *et al.*, "Direct-write bioprinting of cell-laden methacrylated gelatin hydrogels," *Biofabrication*, vol. 6, no. 2, p. 024105, Apr. 2014, doi: 10.1088/1758-5082/6/2/024105.
[44] N. E. Fedorovich, M. H. Oudshoorn, D. van Geemen, W. E. Hennink, J. Alblas, and W. J. A. Dhert, "The effect of photopolymerization on stem cells embedded in hydrogels," *Biomaterials*, vol. 30, no. 3, pp. 344–353, 2009, doi: 10.1016/j.biomaterials.2008.09.037.
[45] S. V. Murphy, A. Skardal, and A. Atala, "Evaluation of hydrogels for bio-printing applications," *Journal of Biomedical Materials Research Part A*, vol. 101A, no. 1, pp. 272–284, Jan. 2013, doi: 10.1002/jbm.a.34326.
[46] D. Loessner *et al.*, "Functionalization, preparation and use of cell-laden gelatin methacryloyl–based hydrogels as modular tissue culture platforms," *Nature Protocols*, vol. 11, no. 4, pp. 727–746, Mar. 2016, doi: 10.1038/nprot.2016.037.
[47] S. Rose *et al.*, "DMSO-free highly differentiated HepaRG spheroids for chronic toxicity, liver functions and genotoxicity studies," *Arch Toxicol*, Nov. 2021, doi: 10.1007/s00204-021-03178-x.
[48] D.-S. Kim *et al.*, "A liver-specific gene expression panel predicts the differentiation status of in vitro hepatocyte models," *Hepatology*, vol. 66, no. 5, pp. 1662–1674, 2017, doi: 10.1002/hep.29324.
[49] J. van der Valk *et al.*, "Fetal bovine serum (FBS): Past – present – future," *ALTEX - Alternatives to animal experimentation*, vol. 35, no. 1, pp. 99–118, Jan. 2018, doi: 10.14573/altex.1705101.
[50] M. D. Burke and R. T. Mayer, "Differential effects of phenobarbitone and 3-methylcholanthrene induction on the hepatic microsomal metabolism and cytochrome P-450-binding of phenoxazone and a homologous series of its n-alkyl ethers (alkoxyresorufins)," *Chemico-Biological Interactions*, vol. 45, no. 2, pp. 243–258, 1983, doi: https://doi.org/10.1016/0009-2797(83)90072-8.
[51] W. Zhu *et al.*, "Direct 3D bioprinting of prevascularized tissue constructs with complex microarchitecture," *Biomaterials*, vol. 124, pp. 106–115, Apr. 2017, doi: 10.1016/j.biomaterials.2017.01.042.
[52] Y.-C. Chen *et al.*, "Functional Human Vascular Network Generated in Photocrosslinkable Gelatin Methacrylate Hydrogels," *Adv. Funct. Mater.*, vol. 22, no. 10, pp. 2027–2039, May 2012, doi: 10.1002/adfm.201101662.
[53] A. K. Miri, H. G. Hosseinabadi, B. Cecen, S. Hassan, and Y. S. Zhang, "Permeability mapping of gelatin methacryloyl hydrogels," *Acta Biomaterialia*, vol. 77, pp. 38–47, Sep. 2018, doi: 10.1016/j.actbio.2018.07.006.
[54] F. Hirschhaeuser, H. Menne, C. Dittfeld, J. West, W. Mueller-Klieser, and L. A. Kunz-Schughart, "Multicellular tumor spheroids: An underestimated tool is catching up again," *Journal of Biotechnology*, vol. 148, no. 1, pp. 3–15, Jul. 2010, doi: 10.1016/j.jbiotec.2010.01.012.
[55] B. Clement, C. Guguen-Guillouzo, J.-P. Campion, D. Glaise, M. Bourel, and A. Guillouzo, "Long-Term Co-Cultures of Adult Human Hepatocytes with Rat Liver Epithelial Cells: Modulation of Albumin Secretion and Accumulation of Extracellular Material," *Hepatology*, vol. 4, no. 3, pp. 373–380, 1984, doi: 10.1002/hep.1840040305.
[56] A. Corlu *et al.*, "A plasma membrane protein is involved in cell contact-mediated regulation of tissue-specific genes in adult hepatocytes.," *The Journal of Cell Biology*, vol. 115, no. 2, pp. 505–515, 1991, doi: 10.1083/jcb.115.2.505.
[57] O. Loréal, F. Levavasseur, C. Fromaget, D. Gros, A. Guillouzo, and B. Clément, "Cooperation of Ito cells and hepatocytes in the deposition of an extracellular matrix in vitro," *The American journal of pathology*, vol. 143, no. 2, pp. 538–544, 1993.
[58] M. Nagaoka, H. Ise, and T. Akaike, "Immobilized E-Cadherin model can enhance cell attachment and differentiation of primary hepatocytes but not proliferation," *Biotechnology Letters*, vol. 24, no. 22, pp. 1857–1862, Nov. 2002, doi: 10.1023/A:1020905532227.
[59] N. Oliva-Vilarnau, S. U. Vorrink, M. Ingelman-Sundberg, and V. M. Lauschke, "A 3D Cell Culture Model Identifies Wnt/ β -Catenin Mediated Inhibition of p53 as a Critical Step during Human Hepatocyte Regeneration," *Adv. Sci.*, vol. 7, no. 15, p. 2000248, Aug. 2020, doi: 10.1002/advs.202000248.
[60] K. Kang *et al.*, "Three-Dimensional Bioprinting of Hepatic Structures with Directly Converted Hepatocyte-Like Cells," *Tissue Engineering Part A*, vol. 24, no. 7–8, pp. 576–583, Apr. 2018, doi: 10.1089/ten.tea.2017.0161.
[61] L. Yang, S. V. Shridhar, M. Gerwitz, and P. Soman, "An in vitro vascular chip using 3D printing-enabled

hydrogel casting," *Biofabrication*, vol. 8, no. 3, p. 035015, Aug. 2016, doi: 10.1088/1758-5090/8/3/035015.
[62] J. Cui, H. Wang, Q. Shi, T. Sun, Q. Huang, and T. Fukuda, "Multicellular Co-Culture in Three-Dimensional Gelatin Methacryloyl Hydrogels for Liver Tissue Engineering," *Molecules*, vol. 24, no. 9, p. 1762, May 2019, doi: 10.3390/molecules24091762.
[63] R. Chang, K. Emami, H. Wu, and W. Sun, "Biofabrication of a three-dimensional liver micro-organ as an in vitro drug metabolism model," *Biofabrication*, vol. 2, no. 4, p. 045004, Dec. 2010, doi: 10.1088/1758-5082/2/4/045004.
[64] Y. Koui *et al.*, "An In Vitro Human Liver Model by iPSC-Derived Parenchymal and Non-parenchymal Cells," *Stem Cell Reports*, vol. 9, no. 2, pp. 490–498, Aug. 2017, doi: 10.1016/j.stemcr.2017.06.010.
[65] L. J. Nelson *et al.*, "Acetaminophen cytotoxicity is ameliorated in a human liver organotypic co-culture model," *Scientific Reports*, vol. 5, no. 1, p. 17455, 2015.

